THE JOURNAL OF PHYSICAL CHEMISTRY LETTERS
A JOURNAL OF THE AMERICAN CHEMICAL SOCIETY

pubs.acs.org/JPCL Letter

Anion Exchange Doping: Tuning Equilibrium to Increase Doping Efficiency in Semiconducting Polymers

Tucker L. Murrey, Margaret A. Riley, Goktug Gonel, Dexter D. Antonio, Leah Filardi, Nikolay Shevchenko, Mark Mascal, and Adam J. Moulé*

Cite This: J. Phys. Chem. Lett. 2021, 12, 1284–1289 Read Online

ACCESS | Metrics & More | Article Recommendations | Supporting Information

ABSTRACT: High electron affinity (EA) molecules p-type dope low ionization energy (IE) polymers, resulting in an equilibrium doping level based on the energetic driving force (IE-EA), reorganization energy, and dopant concentration. Anion exchange doping (AED) is a process whereby the dopant anion is exchanged with a stable ion from an electrolyte. We show that the AED level can be predicted using an isotherm equilibrium model. The exchange of the dopant anion ($FeCl_3^-$) for a bis(trifluoromethanesulfonamide) ($TFSI^-$) anion in the polymers poly(3-hexylthiophene-2,5-diyl) (P3HT) and poly[3-(2,2-bithien-5-yl)-2,5-bis(2-hexyldecyl)-2,5-dihydropyrrolo[3,4-*c*]pyrrole-1,4-dione-6,5-diyl] (PDPP-2T) highlights two cases in which the process is nonspontaneous and spontaneous, respectively. For P3HT, $FeCl_3$ provides a high doping level but an unstable counterion, so exchange results in an air stable counterion with a marginal increase in doping. For PDPP-2T, $FeCl_3$ is a weak dopant, but the exchange of $FeCl_3^-$ for $TFSI^-$ is spontaneous, so the doping level increases by >10× with AED.

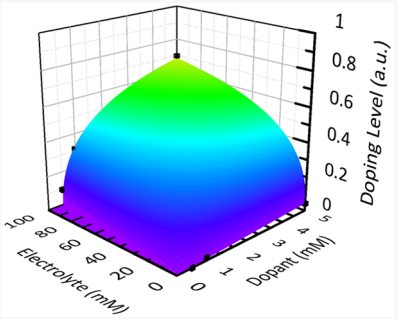

Downloaded via UNIV OF CALIFORNIA DAVIS on February 23, 2021 at 18:02:29 (UTC).
See https://pubs.acs.org/sharingguidelines for options on how to legitimately share published articles.

Sequential doping of semiconducting polymers (SPs) is a well studied method for tuning SP film conductivity and solubility while maintaining a film morphology that is ideal for efficient charge transport.[1−4] Multiple studies have demonstrated that morphology control and sequential doping are essential for obtaining efficient electronic devices, including organic thermoelectrics, organic field effect transistors, and organic electrochemical transistors.[5−9] Recently, Yamashita et al. demonstrated an improvement to molecular doping efficiency through a process termed anion exchange doping (AED).[10] By immersing a poly(2,5-bis(3-tetradecylthiophen-2-yl)thieno[3,2-*b*]thiophene) (PBTTT) film into a solution with the molecular dopant 2,3,5,6-tetrafluoro-7,7,8,8-tetracyanoquinodimethane (F4TCNQ) and various electrolytes, they sequentially doped the polymer and exchanged the $F4TCNQ^-$ anion for the electrolyte anion. This process yields two advantages. First, the anion exchange enables the choice of a stable counterion. Common p-type dopant anions often react with H_2O and O_2. Thus, AED can be used to create air stable films. Second, AED enables increased film dopant levels compared to conventional doping.[10,11] Although AED yields significant advantages, there are fundamental knowledge gaps. Currently, there is no method for predicting the equilibrium doping level or the fraction of exchanged anions. Likewise, the link between doping level and carrier density is poorly understood.

In this manuscript, first we study the relationship between solution concentrations of molecular dopants and electrolyte ions on the P3HT film doping level using the dopant $FeCl_3$ and electrolyte lithium bis(trifluoromethanesulfonyl)imide (LiTFSI), as developed by Jacobs et al.[11] We derive a novel anion exchange isotherm to model equilibrium processes occurring during AED and extract equilibrium constants for both doping and the subsequent anion exchange. This model predicts high p-type doping efficiency is possible in systems with low chemical potential for doping. P-type doping high IE polymers has previously been limited by inherent challenges in the synthesis of stable, high EA dopants.[1,12] By optimizing the AED process, we reduce the need to develop stable, high EA dopants. We demonstrate that high doping levels are achieved using AED with the high IE donor−acceptor polymer poly[3-(2,2-bithien-5-yl)-2,5-bis(2-hexyldecyl)-2,5-dihydropyrrolo-[3,4-*c*]pyrrole-1,4-dione- 6,5-diyl] (PDPP-2T).

Figure 1(a)−(c) illustrates the two equilibrium processes occurring during AED. The Langmuir model, when applied to sequential doping, assumes a fixed and finite number of polymer sites are available for doping and simplifies the complex morphologies present in solid state SPs by assuming that all sites have an identical energy landscape. In reality, solid state P3HT contains crystalline and amorphous regions with a variety of configurations. In Figure 1(a), a 180 nm thick P3HT film is immersed in an 8 mL solution of 5 mM $FeCl_3$ in

Received: December 8, 2020
Accepted: January 19, 2021
Published: January 26, 2021

ACS Publications © 2021 American Chemical Society

https://dx.doi.org/10.1021/acs.jpclett.0c03620
J. Phys. Chem. Lett. 2021, 12, 1284−1289

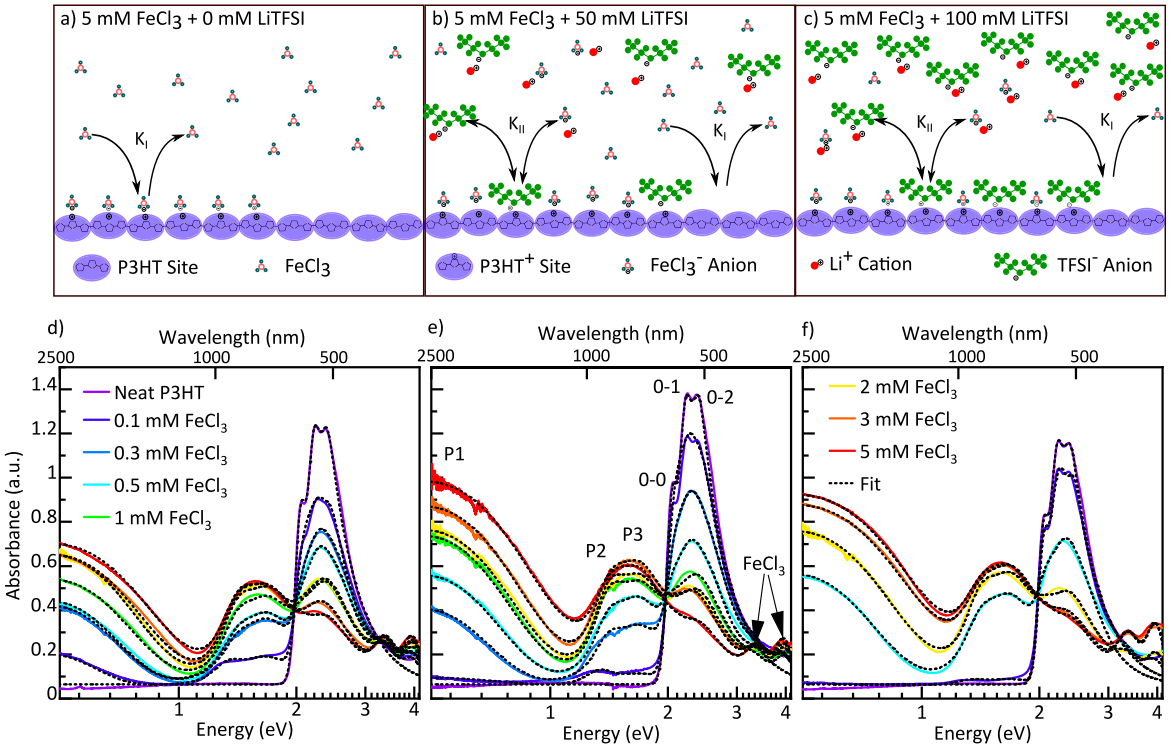

Figure 1. (a) Illustration of $FeCl_3$ doping P3HT sites with equilibrium constant K_I. (b) and (c) illustrate $FeCl_3$ doping P3HT sites, where $FeCl_3^-$ is subsequently exchanged by $TFSI^-$ with equilibrium constant K_{II}. UV−vis−NIR absorption spectra for P3HT films doped with various $FeCl_3$ solution concentrations and (d) 0, (e) 50, and (f) 100 mM LiTFSI solutions, respectively.

anhydrous *n*-butyl acetate (nBA). The solvent swells the film allowing $FeCl_3$ to penetrate and undergo charge transfer with P3HT resulting in $P3HT^+FeCl_3^-$, with equilibrium constant K_I (eq S3).[4] In Figure 1(b),(c), a P3HT film is immersed in 8 mL of 5 mM $FeCl_3$ nBA solution, this time with either 50 mM or 100 mM LiTFSI concentrations, respectively. LiTFSI dissociates into Li^+ and $TFSI^-$ in nBA. $FeCl_3$ dopes the film with the same equilibrium constant; however, the charged $FeCl_3^-$ anion is now exchanged for the $TFSI^-$ anion with an equilibrium constant K_{II} (Equation S4). LiTFSI is inert toward P3HT, so no third equilibrium is required.

$$P3HT^{(SS)} + FeCl_3^{(Sol.)} \rightleftharpoons P3HT^+/FeCl_3^{-(SS)} \quad (1)$$

$$P3HT^+/FeCl_3^{-(SS)} + TFSI^{-(Sol.)} + Li^{+(Sol.)} \rightleftharpoons P3HT^+/TFSI^{-(SS)} + FeCl_3^{-(Sol.)} + Li^{+(Sol.)} \quad (2)$$

Figure 1d shows ultraviolet−visible−near-infrared spectroscopy (UV−vis−NIR) of sequentially doped P3HT films[2,3] with various $FeCl_3$ solutions. Neat P3HT shows three vibronic transitions at ∼2 eV (0−0), ∼2.2 eV (0−1), and ∼2.4 eV (0−2) in accordance with the literature.[13] As P3HT is doped to higher doping levels, the neat 0−0, 0−1, and 0−2 peaks bleach and broaden, while three broad $P3HT^+$ absorbance peaks grow in at 0.47 (P1), 1.25 (P2), and 1.5 (P3) eV.[14−17] As the doping level is increased, an $FeCl_3$ peak becomes apparent at ∼3.9 eV, and an $FeCl_3^-$ peak appears at ∼3.4 eV.[18] UV−vis−NIR of P3HT films sequentially doped with mixtures of $FeCl_3$ and 50 or 100 mM LiTFSI shows similar trends (Figure 1e,f). Key differences are observed in the extent of bleaching of the neat P3HT vibronic transitions and corresponding growth of the broad $P3HT^+$ polaron peaks (P1, P2, and P3) with anion exchanged films yielding a 10−50% higher doping level with respect to $FeCl_3$ solutions without an electrolyte present.

Since the P3 absorbance at 1.5 eV (780 nm) overlaps the neutral P3HT absorbance, we deconvoluted overlapping peaks by globally fitting the spectral signatures between 0.5 and 4.2 eV. The cumulative fits for the 0, 50, and 100 mM LiTFSI series are shown in Figure 1(d)−(f), and their corresponding individual peak fits and the remaining fits for the 0.1, 1.0, 10.0, 25.0, and 75.0 mM LiTFSI concentrations are in Figures S2−S9. Similar to previous studies,[16] we constrained the peak positions to remain constant across all studied samples. Our discussion of the UV−vis−NIR peak fitting is in Supporting Information Section S4.

To simplify these spectral changes with respect to doping level, we define Θ as the fraction of doped P3HT sites over the total available P3HT sites. Θ is linearly approximated from optical absorbance by $\theta = \frac{A_P}{A_P + A_N}$, where A_N is the integral of the neutral P3HT absorption peaks and A_P is the integral of P1. The calculated Θ from the UV−vis−NIR data is shown in Figure 2(a),(b). In films sequentially doped with a 5 mM $FeCl_3$ concentration and no LiTFSI present, 63 ± 3% of the polymer sites are doped (Θ = 0.63 ± 0.03). As the LiTFSI concentration increases to 100 mM at a constant 5 mM $FeCl_3$ concentration, the doping level increases to 75% (Θ = 0.75 ± 0.04).

To determine the equilibrium coefficients K_I and K_{II}, we derive a generalized anion exchange isotherm (eq 3) in terms of known quantities. This model represents the fraction of doped sites over total sites (Θ) for a polymer undergoing charge transfer with a molecular dopant, followed by a subsequent exchange of anions with a monovalent electrolyte. Further description of the extracted Θ and isotherm

https://dx.doi.org/10.1021/acs.jpclett.0c03620
J. Phys. Chem. Lett. 2021, 12, 1284−1289

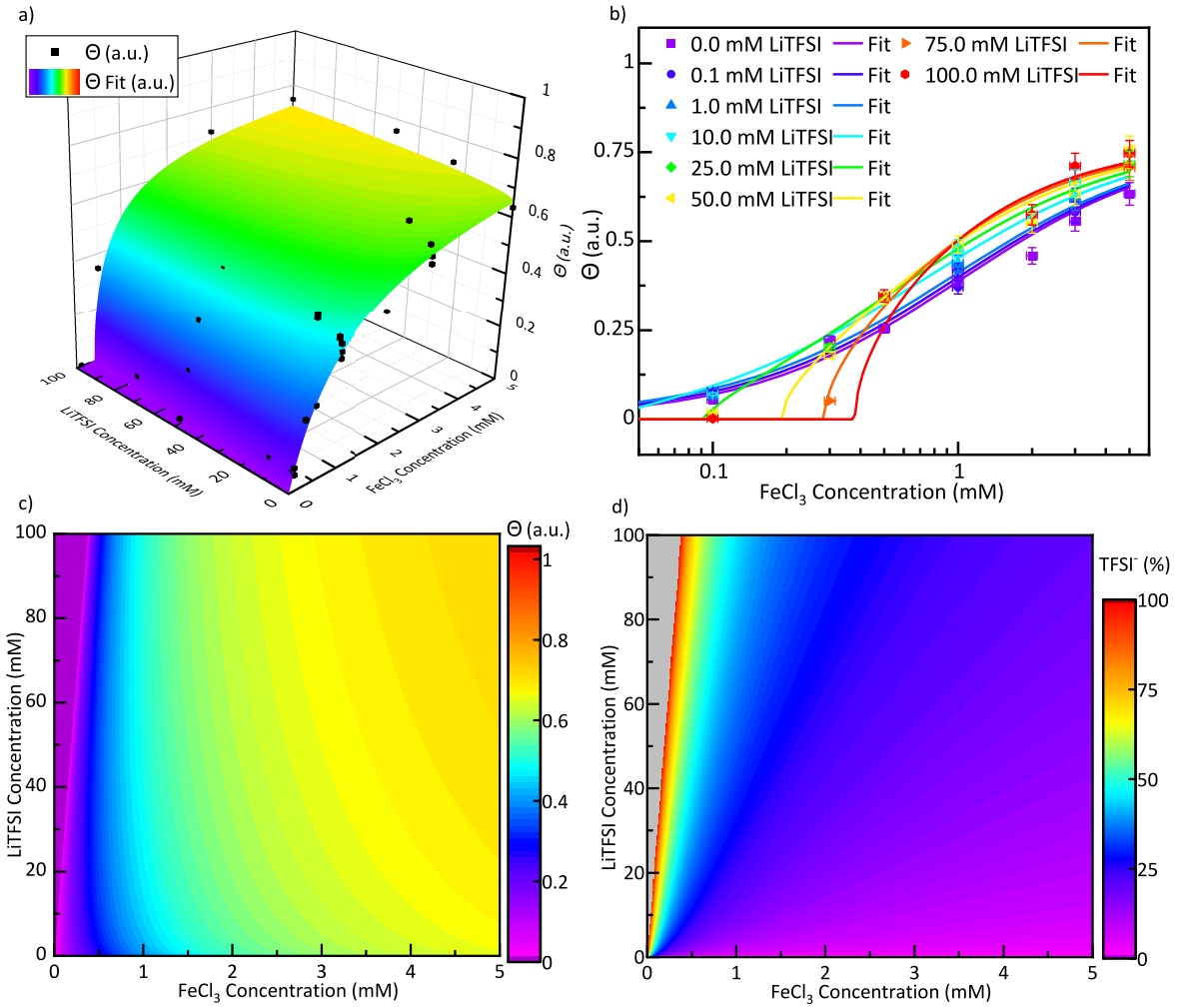

Figure 2. (a) 3D and (b) 2D scatter plots of Θ extracted from UV−vis−NIR and the corresponding anion exchange isotherm fit; (c) shows the Θ fit contour with respect to the prepared $FeCl_3$ and LiTFSI concentrations, and (d) depicts the percentage of doped P3HT sites with $TFSI^-$ anions. The gray region in (d) corresponds to the range in which no P3HT sites are doped.

parameters are in Supporting Information Section S6. The isotherm derivation is in the Supporting Information eqs S3−S25.

$$\Theta = S\frac{K_I([D]-w[C^+A^-]) + \frac{K_IK_{II}([D]-w[C^+A^-])([C^+A^-]-w[C^+A^-])}{\Theta C_t^0 - K_I([D]-w[C^+A^-])(1-\Theta)C_t^0}}{1 + K_I([D]-w[C^+A^-]) + \frac{K_IK_{II}([D]-w[C^+A^-])([C^+A^-]-w[C^+A^-])}{\Theta C_t^0 - K_I([D]-w[C^+A^-])(1-\Theta)C_t^0}} \quad (3)$$

The anion exchange isotherm was fit to the concentration dependent data.[19,20] The best fit is shown in Figure 2a,b, with residuals displayed in Figure S13. The extracted K_I and K_{II} are 971 ± 85 and 0.2 ± 0.06 M^{-1} corresponding to ΔG_I° and ΔG_{II}° of −0.177 ± 0.002 and 0.04 ± 0.007 eV, respectively. As expected, charge transfer between $FeCl_3$ and P3HT is spontaneous. At room temperature, the anion exchange process is nonspontaneous, but a new equilibrium is established between $FeCl_3^-$ and $LiTFSI^-$ counterions. Figure 2c shows the contour of the anion exchange isotherm fit. Θ reduces to zero at low $FeCl_3$ and high LiTFSI concentrations, because the water contamination ($w = 0.0038 \pm 2.3 * 10^{-4}$) exceeds the prepared $FeCl_3$ concentration. At the maximum combined dopant/electrolyte concentrations of 5 mM $FeCl_3$ and 100 mM LiTFSI, the calculated Θ approaches a saturation doping level of 79%, meaning that ∼20% of the neutral P3HT sites cannot be sequentially doped, likely due to disordered dihedral bends along the polymer backbone and/or excluded volume interactions at the substrate or air interfaces. The percent of doped sites occupied by $TFSI^-$ is shown in Figure 2d. Interestingly, in films exposed to 100 mM LiTFSI solutions, the percent of sites with $TFSI^-$ anions remains below ∼50% for all $FeCl_3$ concentrations above ∼1 mM. At 1 mM $FeCl_3$ and 100 mM LiTFSI, approximately half of the doped sites are occupied by $TFSI^-$.

Figure S18 demonstrates that AED can be used to effectively dope SPs with a relatively weak chemical potential for doping. We tested this prediction by attempting the doping of PDPP-2T with $FeCl_3$ in the presence of LiTFSI. PDPP-2T has a higher IE (IE^{CV} = 5.4 eV)[21] than P3HT (IE^{CV} = 5.0 eV), reducing the chemical potential for doping with $FeCl_3$. As a result, doping PDPP-2T with $FeCl_3$ yields low doping efficiency. Figure 3(a) shows raw unnormalized UV−vis−NIR of 80 ± 5 nm thick PDPP-2T films sequentially doped at room temperature with 0.5, 1, and 5 mM $FeCl_3$ solutions. As the doping level is increased, the neutral vibronic (0−0) and (0−1) transitions at 1.3 and 1.5 eV slightly bleach, and polaron transitions P1, P2, and P3 grow in at 0.33, 0.75, and 0.98 eV. An unknown feature grows in with increasing $FeCl_3$ concentration at 1.13 eV; this is discussed in Supporting

https://dx.doi.org/10.1021/acs.jpclett.0c03620
J. Phys. Chem. Lett. 2021, 12, 1284−1289

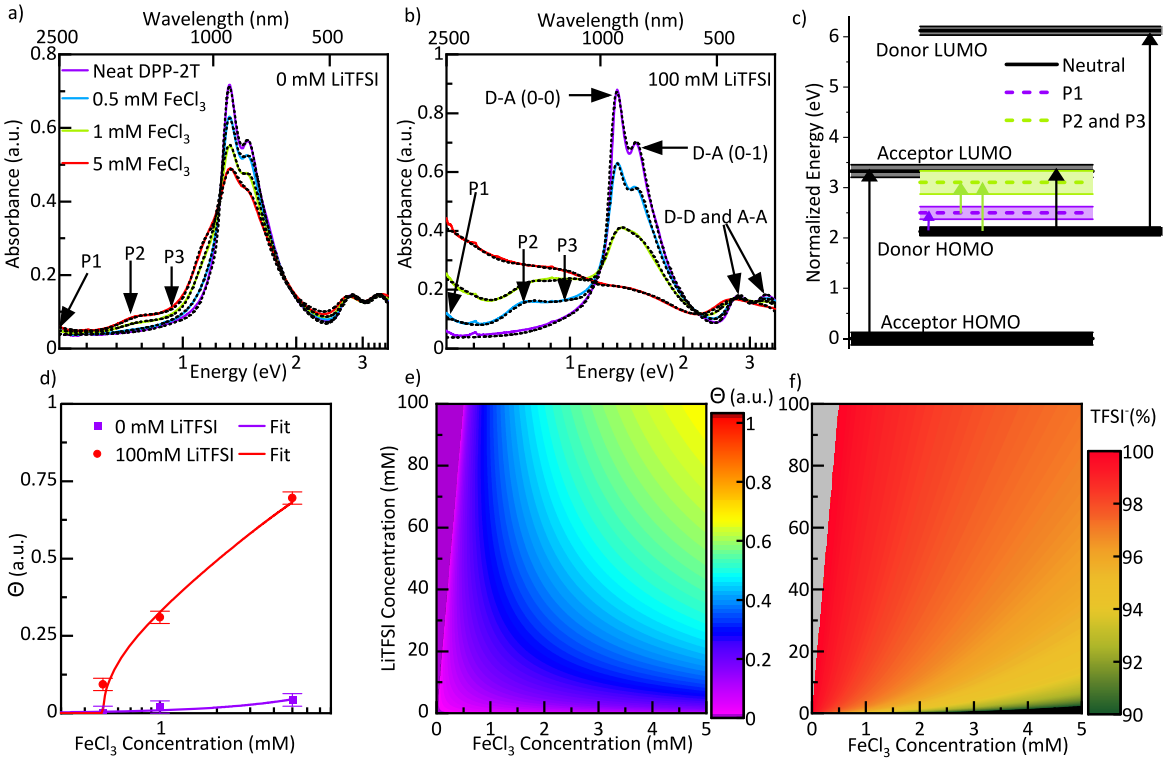

Figure 3. UV−vis−NIR absorption spectra of PDPP-2T films sequentially doped with varying $FeCl_3$ concentrations and either 0 (a) or 100 mM (b) of LiTFSI. All spectra are fit with with cumulative Gaussian fits (dashed lines) to determine state populations. (c) depicts energy transitions for p-doped alternating D/A copolymers. (d) depicts a 2D scatter plot of Θ extracted from the absorption data and the corresponding anion exchange isotherm fit. (e) shows fit Θ for PDPP-2T as a function of the $FeCl_3$ and LiTFSI concentrations, and (f) depicts the percentage of doped polymer sites with $TFSI^-$ anions. The gray region in (f) corresponds to the range in which no polymer sites are doped.

Information Section S5. The two high energy D−D and A−A transitions at 2.8 and 3.3 eV mildly broaden. On the other hand, Figure 3(b) shows UV−vis−NIR of PDPP-2T films sequentially doped with the same 0.5, 1, and 5 mM $FeCl_3$ with the addition of 100 mM LiTFSI. The D−A (0−0) and (0−1) transitions bleach more significantly, and only the P1, P2, and P3 polaron transitions grow in. At the highest doping level, the high energy D−D and A−A transitions quench and broaden, with an increased red-shifted absorbance. Figure 3(c) depicts the corresponding energy transitions.

Discussion of the spectral and isotherm fitting of PDPP-2T is in Supporting Information Section S6.1. The cumulative fits are shown as the dashed line in Figure 3(a),(b). We calculate Θ from the absorption data (Figure 3(d)). As expected, with no LiTFSI present, the higher energetic barrier for charge transfer limits the doping efficiency, reaching a 4.3% doping level ($\theta = 0.043$) with a 5 mM $FeCl_3$ solution. However, in the presence of 100 mM LiTFSI, PDPP-2T reached a 70% doping level ($\theta = 0.70$) at 5 mM $FeCl_3$. We fit Θ for the PDPP-2T samples with the anion exchange isotherm model (Figure 3(d), (e)). The extracted K_I and K_{II} are 9.41 ± 1.62 and 2.92 ± 0.61 M^{-1} corresponding to ΔG_I° and ΔG_{II}° of −0.058 ± 0.004 and −0.028 ± 0.005 eV, respectively. Unlike P3HT, PDPP-2T approaches a saturated doping level of ∼100%. Figure 3(f) shows the calculated % $TFSI^-$ anions in the PDPP-2T film after AED. Unlike the P3HT sample, >90% of doped sites have exchanged $FeCl_3^-$ with $TFSI^-$.

We performed four-point probe collinear sheet resistance measurements on P3HT films with respect to $FeCl_3$ concentration at various LiTFSI concentrations (Figure 4(a)). P3HT films doped with only $FeCl_3$ ranged in conductivity from 0.066 ± 0.002 S/cm at 0.1 mM $FeCl_3$ up to 140 ± 20 S/cm at 5 mM $FeCl_3$. Anion exchanged P3HT films doped with 0.1 mM $FeCl_3$ and 100 mM LiTFSI have the lowest conductivity at $\sim 10^{-3}$ S/cm, due to traces of water in LiTFSI. The presence of LiTFSI led to the largest enhancement in conductivity at 1 mM $FeCl_3$, where the measured conductivity increased from 31 ± 6 S/cm at 0 mM LiTFSI to 80 ± 6 S/cm at 100 mM LiTFSI. For this sample, 43% of the $P3HT^+$ sites have $TFSI^-$ and 57% have $FeCl_3^-$ counterions. Discussion of conductivity enhancement is in Supporting Information Section S13.

Carrier density is proportional to the fraction of polymer sites that possess a hole (Θ). To estimate the hole density from Θ, we estimate the minimum site size, which we define as the minimum number of monomer units that can hold a hole state. For the PDPP-2T polymer, we assume that each monomer T-DPP-T is a single site. This assumption is justified by recent first-principle simulations of alternating copolymers.[22] Using a film density of 1.1 g/cm^3, we estimate a maximum hole density (p_{max}) of 8.2 × 10^{20} holes/cm^3 for PDPP-2T. A 10% uncertainty in film mass density translates to a 10% uncertainty in maximum carrier density. For P3HT, we assume the minimum site size is a four thiophene (4T) monomer section and yields an estimated maximum hole density of 8.5 × 10^{20} holes/cm^3, nearly identical to that of PDPP-2T. We recognize that more accurate estimates of the minimum site size and maximum carrier density will improve our model's predictive power. Discussion of carrier density is in Supporting Information Section S14.

https://dx.doi.org/10.1021/acs.jpclett.0c03620
J. Phys. Chem. Lett. 2021, 12, 1284−1289

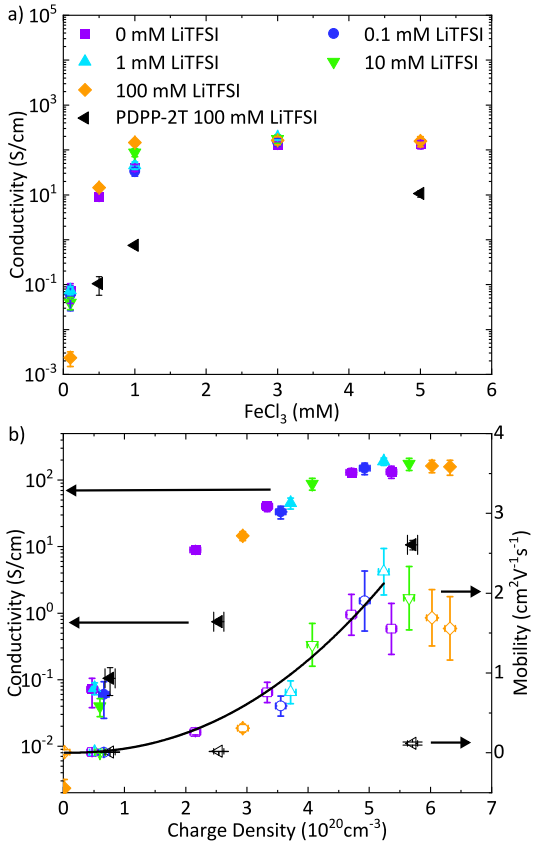

Figure 4. (a) Four-point probe conductivity of P3HT films with respect to $FeCl_3$ solution concentration at various LiTFSI concentrations, and one conductivity series of PDPP-2T films with respect to $FeCl_3$ solution concentrations with 100 mM LiTFSI. (b) Conductivity (filled symbols) and mobility (empty symbols) as a function of charge density.

Scaling these maximum hole densities by the fraction of sites that are doped (Θ) allows us to compare film conductivity (σ) to hole density and estimate hole mobility (eq 4)

$$\mu = \frac{\sigma}{p_{max}\Theta e} \tag{4}$$

where e is the elemental charge (Figure 4(b)). The P3HT hole mobility is fit to the variable range hopping model (VRHM) (Equation S27),[23−25] where the prefactor for conductivity (σ_0 = 1.6 S/m), the effective overlap parameter between localized states (α^{-1} = 0.16 nm), and the critical number for the onset of percolation (B_c = 2.8) are identical to those of previous P3HT mobility studies.[23,26] Our sample has an increased width of the exponential density of states (T_0 = 665 K) compared to previous fits to P3HT. This analysis shows that μ_h increases with doping density until it saturates at 2.3 $cm^2\ V^{-1}\ s^{-1}$ at a doping density of ~5 × 10^{20} cm^{-3}. At higher doping levels, μ_h deviates from the VRHM due to increased structural disorder induced by the presence of counterions.[8]

We were unable to measure the conductivity of the PDPP-2T films doped with only $FeCl_3$, because it was below the detection limit of our equipment (<10^{-3} S/cm). The conductivity of PDPP-2T films anion exchange doped at 100 mM LiTFSI ranged from 0.1 ± 0.05 S/cm with 0.5 mM $FeCl_3$ up to 10.7 ± 1.8 S/cm with 5 mM $FeCl_3$ (Figure 4 (a)). IV curves are in Figure S22. The estimated hole density and mobility are in Figure 4(b). The estimated PDPP-2T mobility increased from 0.009 to 0.117 $cm^2\ V^{-1}\ s^{-1}$ at 0.5 mM and 5 mM $FeCl_3$, respectively.

In summary, we demonstrate sequential AED of P3HT and PDPP-2T films with the dopant $FeCl_3$ and electrolyte LiTFSI. In P3HT, AED is nonspontaneous, and doping efficiency increases by 10 to 50% in the presence of LiTFSI. We demonstrate control over the exchange of $FeCl_3^-$ for $TFSI^-$ on $P3HT^+$ sites between 0 and 100%. Sheet resistance measurements reveal record P3HT film conductivities of ~140 S/cm can be obtained at high $FeCl_3$ doping levels and remain the same in AED P3HT. In PDPP-2T, AED is spontaneous, doping efficiency increases >10× in the presence of LiTFSI, and conductivity increases by >4 orders of magnitude. Therefore, AED enables high p-type doping efficiency in systems with low chemical potential for doping. Future research is needed on AED polymers to address the effects that anion exchange has on polaron delocalization, the stability of doping density in the presence of external stimuli, and how anion exchange affects the polymer film morphology.

■ ASSOCIATED CONTENT

Supporting Information

The Supporting Information is available free of charge at https://pubs.acs.org/doi/10.1021/acs.jpclett.0c03620.

Molecular Structure of Materials, Experimental Methods, PDPP-2T Synthesis, UV−vis−NIR Full Gaussian Fits, PDPP-2T $FeCl_3$ Absorption Discussion, Fractional Doping Level (Θ) and Isotherm Fitting, Discussion of $\Delta G°$, P3HT Anion Exchange (Assuming one monomer site), Anion Exchange Isotherm Site Size Comparison, Discussion of Θ: Is $\Theta \propto$ P1 or $\propto \sum$(P1, P2, P3)?, Anion Exchange Simulations, Extra UV−vis−NIR Tests, Sheet Resistance IV Curves and Discussion of Conductivity Enhancements, Discussion of Carrier Density, X-ray Photoelectron Spectroscopy (PDF)

■ AUTHOR INFORMATION

Corresponding Author

Adam J. Moulé − *Department of Chemical Engineering, University of California, Davis, Davis, California 95616, United States;* orcid.org/0000-0003-1354-3517; Email: amoule@ucdavis.edu

Authors

Tucker L. Murrey − *Department of Material Science and Engineering, University of California, Davis, Davis, California 95616, United States;* orcid.org/0000-0002-5947-2892

Margaret A. Riley − *Department of Chemical Engineering, University of California, Davis, Davis, California 95616, United States*

Goktug Gonel − *Department of Chemical Engineering, University of California, Davis, Davis, California 95616, United States*

Dexter D. Antonio − *Department of Chemical Engineering, University of California, Davis, Davis, California 95616, United States*

Leah Filardi − *Department of Chemical Engineering, University of California, Davis, Davis, California 95616, United States;* orcid.org/0000-0002-0271-7879

Nikolay Shevchenko − *Department of Chemistry, University of California, Davis, Davis, California 95616, United States*

https://dx.doi.org/10.1021/acs.jpclett.0c03620
J. Phys. Chem. Lett. 2021, 12, 1284−1289

Mark Mascal − *Department of Chemistry, University of California, Davis, Davis, California 95616, United States;* orcid.org/0000-0001-7841-253X

Complete contact information is available at: https://pubs.acs.org/10.1021/acs.jpclett.0c03620

Notes

The authors declare no competing financial interest.

■ ACKNOWLEDGMENTS

This research was funded by the National Science Foundation Scalable Nanomanufacturing Program, Award # CMMI 1636385. We thank the National Science Foundation Division of Materials Research (award no. MRI-182838) for funding the acquisition of the XPS instrument used in this work and Ian Jacobs for helping with dopant formulation and processing techniques.

■ REFERENCES

(1) Jacobs, I. E.; Moulé, A. J. Controlling Molecular Doping in Organic Semiconductors. *Adv. Mater.* **2017**, *29*, 1703063.

(2) Jacobs, I. E.; Aasen, E. W.; Oliveira, J. L.; Fonseca, T. N.; Roehling, J. D.; Li, J.; Zhang, G.; Augustine, M. P.; Mascal, M.; Moulé, A. J. Comparison of Solution-Mixed and Sequentially Processed P3HT:F4TCNQ Films: Effect of Doping-Induced Aggregation on Film Morphology. *J. Mater. Chem. C* **2016**, *4*, 3454−3466.

(3) Scholes, D. T.; Yee, P. Y.; Lindemuth, J. R.; Kang, H.; Onorato, J.; Ghosh, R.; Luscombe, C. K.; Spano, F. C.; Tolbert, S. H.; Schwartz, B. J. The Effects of Crystallinity on Charge Transport and the Structure of Sequentially Processed F4TCNQ-Doped Conjugated Polymer Films. *Adv. Funct. Mater.* **2017**, *27*, 1702654.

(4) Murrey, T. L.; Guo, K.; Mulvey, J. T.; Lee, O. A.; Cendra, C.; Bedolla-Valdez, Z. I.; Salleo, A.; Moulin, J.-F.; Hong, K.; Moulé, A. J. Additive Solution Deposition of Multi-Layered Semiconducting Polymer Films for Design of Sophisticated Device Architectures. *J. Mater. Chem. C* **2019**, *7*, 953−960.

(5) Patel, S. N.; Glaudell, A. M.; Peterson, K. A.; Thomas, E. M.; O'Hara, K. A.; Lim, E.; Chabinyc, M. L. Morphology Controls the Thermoelectric Power Factor of a Doped Semiconducting Polymer. *Sci. Adv.* **2017**, *3*, No. e1700434.

(6) Hofmann, A. I.; Kroon, R.; Zokaei, S.; Järsvall, E.; Malacrida, C.; Ludwigs, S.; Biskup, T.; Müller, C. Chemical Doping of Conjugated Polymers with the Strong Oxidant Magic Blue. *Adv. Electron. Mater.* **2020**, *6*, 2000249.

(7) Kang, K.; Watanabe, S.; Broch, K.; Sepe, A.; Brown, A.; Nasrallah, I.; Nikolka, M.; Fei, Z.; Heeney, M.; Matsumoto, D.; et al. 2D Coherent Charge Transport in Highly OrderedConducting Polymers Doped by Solid StateDiffusion. *Nat. Mater.* **2016**, *15*, 896−902.

(8) Fratini, S.; Nikolka, M.; Salleo, A.; Schweicher, G.; Sirringhaus, H. Charge Transport in High-Mobility Conjugated Polymers and Molecular Semiconductors. *Nat. Mater.* **2020**, *19*, 491−502.

(9) Rivnay, J.; Inal, S.; Salleo, A.; Owens, R. M.; Berggren, M.; Malliaras, G. G. Organic Electrochemical Transistors. *Nat. Rev. Mater.* **2018**, *3*, 17086.

(10) Yamashita, Y.; Tsurumi, J.; Ohno, M.; Fujimoto, R.; Kumagai, S.; Kurosawa, T.; Okamoto, T.; Takeya, J.; Watanabe, S. Efficient Molecular Doping of Polymeric Semiconductors Driven by Anion Exchange. *Nature* **2019**, *572*, 634−638.

(11) Jacobs, I. E.; D'Avino, G.; Lin, Y.; Lemaur, V.; Huang, Y.; Ren, X.; Simatos, D.; Wood, W.; Chen, C.; Harrelson, T.; et al. Ion-Exchange Doped Polymers at the Degenerate Limit: What Limits Conductivity at 100% Doping Efficiency? *arXiv* 2021.

(12) Lüssem, B.; Keum, C.-M.; Kasemann, D.; Naab, B.; Bao, Z.; Leo, K. Doped Organic Transistors. *Chem. Rev.* **2016**, *116*, 13714−13751.

(13) Rahimi, K.; Botiz, I.; Agumba, J. O.; Motamen, S.; Stingelin, N.; Reiter, G. Light Absorption of Poly(3-hexylthiophene) Single Crystals. *RSC Adv.* **2014**, *4*, 11121−11123.

(14) Österbacka, R.; An, C. P.; Jiang, X. M.; Vardeny, Z. V. Two-Dimensional Electronic Excitations in Self-Assembled Conjugated Polymer Nanocrystals. *Science* **2000**, *287*, 839.

(15) Korovyanko, O. J.; Österbacka, R.; Jiang, X. M.; Vardeny, Z. V.; Janssen, R. A. J. Photoexcitation Dynamics in Regioregular and Regiorandom Polythiophene Films. *Phys. Rev. B: Condens. Matter Mater. Phys.* **2001**, *64*, 235122.

(16) Wang, C.; Duong, D. T.; Vandewal, K.; Rivnay, J.; Salleo, A. Optical Measurement of Doping Efficiency in Poly(3-hexylthiophene) Solutions and Thin Films. *Phys. Rev. B: Condens. Matter Mater. Phys.* **2015**, *91*, No. 085205.

(17) Salzmann, I.; Heimel, G.; Oehzelt, M.; Winkler, S.; Koch, N. Molecular Electrical Doping of Organic Semiconductors: Fundamental Mechanisms and Emerging Dopant Design Rules. *Acc. Chem. Res.* **2016**, *49*, 370−378.

(18) Abderrazak, H.; Dachraoui, M.; Lendl, B. A Novel Flow Injection Procedure for Determination of Phosphate in Industrial Raw Phosphoric Acid. *Analyst* **2000**, *125*, 1211−1213.

(19) Levenberg, K. A Method for the Solution of Certain Non-Linear Problems in Least Squares. *Q. Appl. Math.* **1944**, *2*, 164−168.

(20) Marquardt, D. W. An Algorithm for Least-Squares Estimation of Nonlinear Parameters. *J. Soc. Ind. Appl. Math.* **1963**, *11* (2), 431−441.

(21) Li, Y.; Sun, B.; Sonar, P.; Singh, S. P. Solution Processable Poly(2,5-dialkyl-2,5-dihydro-3,6-di-2-thienyl-pyrrolo[3,4-c]pyrrole-1,4-dione) for Ambipolar Organic Thin Film Transistors. *Org. Electron.* **2012**, *13*, 1606−1613.

(22) Balooch Qarai, M.; Chang, X.; Spano, F. C. Vibronic Exciton Model for Low Bandgap DonorAcceptor Polymers. *J. Chem. Phys.* **2020**, *153*, 244901.

(23) Tanase, C.; Meijer, E. J.; Blom, P. W. M.; de Leeuw, D. M. Unification of the Hole Transport in Polymeric Field-Effect Transistors and Light-Emitting Diodes. *Phys. Rev. Lett.* **2003**, *91*, 216601.

(24) Pasveer, W. F.; Cottaar, J.; Tanase, C.; Coehoorn, R.; Bobbert, P. A.; Blom, P. W. M.; de Leeuw, D. M.; Michels, M. A. J. Unified Description of Charge-Carrier Mobilities in Disordered Semiconducting Polymers. *Phys. Rev. Lett.* **2005**, *94*, 206601.

(25) Vissenberg, M. C. J. M.; Matters, M. Theory of the Field-Effect Mobility in Amorphous Organic Transistors. *Phys. Rev. B: Condens. Matter Mater. Phys.* **1998**, *57*, 12964−12967.

(26) Seager, C. H.; Pike, G. E. Percolation and Conductivity: A Computer Study. II. *Phys. Rev. B* **1974**, *10*, 1435−1446.